

# Spectroscopy of the post-AGB star HD 101584(IRAS 11385-5517) \*

**T. Sivarani<sup>1</sup>, M. Parthasarathy<sup>1</sup>, P. García-Lario<sup>2</sup>, A. Manchado<sup>3</sup>, and S.R. Pottasch<sup>4</sup>**

<sup>1</sup> Indian Institute of Astrophysics, Bangalore 560 034, India.

<sup>2</sup> ISO Data Centre, Astrophysics Division, Space Science Department of ESA, Villafranca del Castillo, Apartado de Correos 50727,28080 Madrid, Spain.

<sup>3</sup> Instituto de Astrofísica de Canarias, E-38200 La Laguna, Tenerife, Spain.

<sup>4</sup> Kapteyn Astronomical Institute, Postbus 800, NL-9700 AV Groningen, The Netherlands.

Received /Accepted

**Abstract.** From an analysis of the spectrum (4000Å to 8800Å) of HD 101584 it is found that most of the neutral and single ionized metallic lines are in emission. The forbidden emission lines of [OI] 6300Å and 6363Å and [CI] 8727Å are detected, which indicate the presence of a very low excitation nebula. The H $\alpha$ , FeII 6383Å, NaI D<sub>1</sub>, D<sub>2</sub> lines and the CaII IR triplet lines show P-Cygni profiles indicating a mass outflow. The H $\alpha$  line shows many velocity components in the profile. The FeII 6383Å also has almost the same line profile as the H $\alpha$  line indicating that they are formed in the same region. From the spectrum synthesis analysis we find the atmospheric parameters to be  $T_{eff}=8500$ K,  $\log g=1.5$ ,  $V_{turb}=13$ km s<sup>-1</sup> and  $[Fe/H]=0.0$ . From an analysis of the absorption lines the photospheric abundances of some of the elements are derived. Carbon and nitrogen are found to be overabundant. From the analysis of Fe emission lines we derived  $T_{ext}=6100$ K $\pm 200$  for the emission line region.

**Key words:** stars: abundances-stars: evolution-stars: supergiants-stars: post-AGB-stars: circumstellar matter-stars: individual: HD 101584

## 1. Introduction

Humphreys and Ney (1974) found near-infrared excess in HD 101584 and suggested that it is a massive F-supergiant with an M-type binary companion star (Humphreys 1976). However, HD 101584 (V=7.01, F0 IaP (Hofleit et al. 1983)) was found to be an IRAS source (IRAS 11385-5517) (Parthasarathy and Pottasch 1986). On the basis of its far-infrared colors, flux distribution and

*Send offprint requests to:* T. Sivarani

\* Based on observations obtained at the European Southern Observatory(ESO), Chile and the Vainu Bappu Observatory, Kavalur, India

*Correspondence to:* sivarani@iias.ernet.in

detached cold circumstellar dust shell, Parthasarathy and Pottasch (1986) suggested that it is a low mass star in the post-Asymptotic Giant Branch (post-AGB) stage of evolution.

CO molecular emission lines at millimeter wavelengths were detected by Trams et al. (1990). The complex structure of the CO emission shows large Doppler velocities of 130 km s<sup>-1</sup> with respect to the central velocity of the feature indicating a very high outflow velocity. Te Lintel Hekkert et al. (1992) reported the discovery of OH 1667 MHz maser emission from the circumstellar envelope of HD 101584. The OH spectrum has a velocity range of 84 km s<sup>-1</sup> and shows two unusually broad emission features. Te Lintel Hekkert et al. (1992) found from the images obtained from the Australian Telescope, that the OH masers are located along the bipolar outflow. The post-AGB nature of HD 101584 is also suggested by the space velocity of the star derived from the central velocity of the CO and OH line emission. This velocity of  $V_{rad}=50.3\pm 2.0$  km s<sup>-1</sup> does not agree with the galactic rotation curve assuming it to be a luminous massive population I F supergiant.

Bakker et al. (1996a) studied the low and high resolution ultraviolet spectra and the high resolution optical spectra of HD 101584. Based on the strength of HeI (see also Morrison and Zimba 1989) N II, C II lines and Geneva photometry, Bakker et al. (1996a) suggest that HD 101584 is a B9 II star of  $T_{eff}=12000$ K $\pm 1000$ K and  $\log g=3.0$ . Bakker et al. (1996b) also found small amplitude light and velocity variations and suggested that HD 101584 is a binary with an orbital period of 218 days.

The optical spectrum of HD 101584 is very complex and shows many lines in emission. In this paper we report an analysis of the high resolution optical spectrum of HD 101584.

## 2. Observations and analysis

High resolution and high signal to noise ratio spectra of HD 101584 were obtained with the European Southern Observatory (ESO) Coude Auxiliary Telescope (CAT) equipped with the Coude Echelle Spectrograph (CES) and a CCD as detector. The spectra cover the wavelength regions 5360-5400Å, 6135-6185Å, 6280-6320Å, 6340-6385Å, 6540-6590Å, 7090-7140Å, 7420-7480Å, 8305-8365Å and 8680-8740Å. The spectral resolution ranged from 0.165Å at 6150Å to 0.210Å at 8700Å. We have also obtained 2.5Å resolution spectra of HD 101584 from 3900Å to 8600Å with the 1m telescope and UAGS spectrograph and a CCD as detector at the Vainu Bappu Observatory (VBO), Kavalur, India. In addition we obtained CCD spectra with the same telescope and Coude Echelle spectrograph, covering the wavelength region 4600Å to 6600Å with a resolution of 0.4Å. All spectra mentioned above were used in this analysis.

All the spectra were analyzed using IRAF software. The equivalent widths of lines were found by fitting a gaussian. For blended lines de-blending was done by fitting multiple gaussians. We carried out spectrum synthesis calculations using KURUCZ stellar models (1994). SYNSPEC code (Hubeny et al. 1985) was used for calculating the theoretical line profiles. The gf values were taken from Wiese et al. (1966), Wiese and Martin (1980), Hibbert et al. (1991), Parthasarathy et al. (1992) and Reddy et al. (1997 and references therein). For the analysis of forbidden lines we have used the IRAF software package NEBULAR under STSDAS.

## 3. Description of the spectrum

The remarkable characteristic of the optical spectrum of HD 101584 is the fact that different spectral regions resemble different spectral types. The spectrum in the UV region is similar to that of  $\alpha$  Lep which is an F-supergiant (Bakker 1994). The optical spectrum in the range 3600Å-5400Å is dominated by absorption lines. Most of them are due to neutral and single ionized lines of Ti, Cr and Fe. The CaII H and K absorption lines are strong. The strength of the absorption lines are similar to that observed in an A2 supergiant. In the yellow and red spectral regions, most of the lines are in emission (Fig. 1). The emission lines show complex line profiles. The absorption lines of NI, OI, CII and SiII are broad. The Paschen lines are in absorption. Some of these absorption lines are blended with emission lines and many have asymmetric profiles. The OI lines at 6156Å are blended with emission lines of FeI. The NI lines are strong and show asymmetric line profiles. The blue wing is shallow compared to the red wing. The CII lines at 6578Å and 6582Å are weak. The Na D lines, KI 7700 Å (Fig. 2), the CaII IR triplet lines (Fig. 3), [OI], [CI] and MgI 6318.7Å lines are found in emission. The OI triplet lines (Fig. 2) are very strong indicating an extended atmosphere and NLTE effects.

### 3.1. P-Cygni profiles

The H $\alpha$  line has a very strong P-Cygni profile indicating an outflow. The profile looks very complex. It shows at least 6 velocity components. The FeII line at 6383Å is in emission and the profile is very similar to that of H $\alpha$  (Fig. 4). Similar behaviour of the 6383Å FeII line and H $\alpha$  line is also noticed in the post-AGB F supergiant IRAS 10215-5916 (García-Lario et al. 1994). The H $\alpha$  and the FeII 6383Å line show an outflow velocity of  $100 \pm 10$  km s $^{-1}$ . The H $\beta$  line also shows a P-Cygni profile. It has a broad emission wing at the red end. This indicates that the line forming region is extended. The H $\beta$ , NaI D1, D2 and the CaII IR triplet lines (Fig. 3) show an outflow velocity of  $75 \pm 20$  km s $^{-1}$ . The velocity structure seen in these P-Cygni profiles could be due to emission from different shells formed during the episodic mass-loss events.

### 3.2. FeI and FeII emission lines

The presence of numerous emission lines of FeI and FeII makes it possible to derive the physical conditions of the line forming region. From the curve of growth analysis of the FeI and FeII emission lines (Viotti 1969), we have derived  $T_{exi}=6300 \pm 1000$ K and  $5550 \pm 1700$ K respectively (Fig. 5). The scatter found could be due to the fact that the lines are not optically thin. On the other hand, there are only few emission lines of FeII present in the spectra and thus the estimate from FeII might not be accurate. In order to determine whether the large scatter observed in Fig. 4 is reflecting optical thickness effects we have done self-absorption curve (SAC) analysis (Friedjung and Murratario 1987) for the FeI emission lines.

SAC is a kind of curve of growth applied to emission lines, but it has certain advantages as compared to the classical emission line curve of growth analysis. This method of analysis is valid also for optically thick lines. It deals with each transition separately, so that it is possible to get the population of different levels without assuming a Boltzmann distribution. In this curve, a function of the line flux emitted in the different transition of a given multiplet is taken in such a way that it is constant for a optically thin uniform medium. As the optical thickness increases the curve will move towards a straight line inclined at -45°. The shape of the SAC in Fig. 6(a) shows the lines are optically thick. The shape of the SAC is obtained by shifting all the multiplets with respect to a reference multiplet. Here we have taken multiplet 207 as reference. The X and Y shifts of each multiplet gives the relative population of the lower and upper level with respect to the reference multiplet. Fig. 6(b) and Fig. 6(c) shows the Y and X shifts versus the upper and lower excitation potential from which we derive the  $T_{exi}=6100 \pm 200$ K.

### 3.3. Forbidden lines

The forbidden emission lines at 5577Å, 6300Å and 6363Å of neutral oxygen are present in the spectra. The forbidden line of neutral carbon at 8727Å is also seen. The 6300Å line is blended with ScII line and the 5577Å line is very weak. We have calculated the  $I(6300)+I(6363)/I(5577)$  to be 13.3. From the flux ratio we can calculate  $T_e$  (Osterbrock 1989). This flux ratio is not very accurate because of very the weak 5577Å line and poor signal to noise spectrum. For the flux ratio of 13.3 we derived a function depending on the electron density  $N_e$  and temperature  $T_e$ . Figure 7 shows the  $N_e$  and  $T_e$  contours for different values of flux ratio around 13.3. Since we do not see any other forbidden lines which are sensitive to the electron density, we could not fix both  $N_e$  and  $T_e$  uniquely. But assuming a temperature derived from the Fe emission lines, an electron density of  $1 \times 10^7$  is obtained. For this value of electron density and temperature the C/O =  $0.5 \pm 0.2$  has been obtained.

## 4. Radial velocities

There are very few absorption lines and most of these are affected by emission and or a shell component, therefore we derived the average radial velocity from the well defined emission lines. The average radial velocity from the emission lines is found to be  $50 \pm 2 \text{ km s}^{-1}$ . Morrison and Zimba (1989) using 14 best absorption lines found the radial velocity to be  $69 \pm 1 \text{ km s}^{-1}$ . From the equivalent widths of FeI absorption lines given by Rosenzweig et al. (1997) we find no correlation between  $\log g_f - \chi\Theta$  and heliocentric radial velocity (Fig. 8). However, Bakker et al. (1996a) found a correlations between  $\log g_f - \chi\Theta$  and heliocentric radial velocities of HD101584 in the UV. The discrepancy could be due to the poor resolution of Rosenzweig et al. (1997) data compared to that of Bakker et al. (1996a). The large scatter seen in the radial velocities could be due to pulsation. Similar velocity variations were noticed in other post-AGB supergiants (García-Lario et al. 1997, Hrivnak 1997).

## 5. Atmospheric parameters and chemical composition

The UV (IUE) low resolution spectrum of HD 101584 matches well with that of an A6Ia star (HD 97534) (Fig. 10) indicating a  $T_{eff}$  of 8400K (Lang 1992). The presence of CII lines at 6578Å and 6582Å indicates a  $T_{eff} > 8000\text{K}$ . For  $T_{eff} \leq 8000\text{K}$  the CII lines would be very weak or absent. The Paschen lines also indicates a low gravity (Fig. 11). The luminosity class Ia also indicates a very low gravity. From the analysis of several nitrogen lines around 7440Å and 8710Å we derived the microturbulence velocity  $V_{turb}=13\text{ km s}^{-1}$ . We synthesised the spectral region from 4000Å to 4700Å (Fig. 9) with low gravity ( $\log g = 1.5$ ) models of Kurucz (1993) with temperatures

8000K, 8500K and 9000K. The best fit was found for  $T_{eff} = 8500\text{K}$ ,  $\log g = 1.5$ ,  $V_T=13\text{ km s}^{-1}$  and  $[\text{Fe}/\text{H}] = 0.0$ .

The line at 5876Å was identified as a HeI line by Bakker et al. (1996a) who also state that the lines at 5047Å and 5045Å as due to HeI and NII respectively. However, we find that the 5047 and 5045 lines are in fact due to FeII. Except HeI 5876Å, we have not found any other helium lines in the spectrum and nor have we found any NII or OII lines. In fact, Hibbert et al. (1991) indicate the presence of a CI line at 5876Å. It is likely that the line at 5876Å may be due to CI instead of HeI.

If we assume that the 5876Å line is due to HeI then for a solar helium abundance and  $\log g = 1.5$ ,  $T_{eff} = 9000\text{K}$  is found. Since we do not see any other helium lines, if 5876Å line is due to helium , it is likely that it may be formed in the stellar wind or in the chromosphere of the star. On the basis of the presence of this helium line Bakker et al. (1996a) suggested that HD 101584 is a B9II star of  $T_{eff} 12000\text{K}$ . On the basis of the analysis of our spectra we have not found any evidence for such a high temperature. We have also analysed the equivalent widths of absorption lines in the spectrum of HD 101584 given by Bakker et al.(1996a). The final abundances of some of the elements are listed in Table 2. The abundances listed in Table 2 show that the star is overabundant in carbon and nitrogen. It appears that the material processed by the triple alpha C-N and O-N cycle has reached the surface.

## 6. Discussion and Conclusions

The optical spectrum of the post-AGB star HD 101584 is rather complex. We find several emission lines and P-Cygni profiles indicating an ongoing mass-loss and the presence of a circumstellar gaseous envelope. From the analysis of the absorption lines we find the atmospheric parameters to be  $T_{eff}=8500\text{K}$  ,  $\log g=1.5$ ,  $V_t=13\text{ km s}^{-1}$  and  $[\text{Fe}/\text{H}]=0.0$ .

Carbon and Nitrogen are found to be overabundant indicating that material processed by triple alpha C-N and O-N cycles has reached the surface. Since our blue spectra are of relatively low resolution and because of the presence of emission and shell components it is difficult to estimate reliable abundances of s-process elements. The OI line at 6156Å is blended with a weak FeI emission line. The OI triplet at 7777Å is very strong and affected by NLTE. In any case it appears that the oxygen abundance is nearly solar. A NLTE analysis of the high resolution OI 7777Å triplet may yield a more reliable oxygen abundance.

The nitrogen abundance is based on 6 lines in the 7440Å and 8710Å region. We have not used the strong nitrogen lines. Nitrogen seems to be clearly overabundant. The carbon abundance is based on two CII lines at 6578Å and 6582Å. There is a clear indication that carbon is overabundant. The abundance of Mg, Ti, and Fe are nearly solar. The Ti abundance is based on 15 lines and the Fe abundance is based on 6 lines. Many of the other atomic

lines are affected by emission and shell components. In our opinion, the line at 5876Å might be due to CI (Hibbert et al. 1991) and not to HeI, as previously suggested by Bakker et al. (1996a). We have not found any other HeI, NII or OII lines. Our analysis shows that the  $T_{eff}$  is  $8500 \pm 500$ K.

Bakker et al. (1996b) found small amplitude light and velocity variations and suggested that HD 101584 is a binary with an orbital period of 218 days. The radial velocity variations may be due to pulsation, macroturbulence motions or shock waves in the outer layers of the stellar atmosphere. Many post-AGB supergiants show small amplitude light and velocity variations (Hrivnak 1997). These variations may not be interpreted as due to the presence of a binary companion. Long term monitoring of the radial velocities is needed in order to understand the causes for these variations.

The spectrum and the brightness of HD 101584 appears to remain the same during last two or three decades. There is no evidence for significant variations in brightness similar to those observed in Luminous Blue Variables (LBVs). The chemical composition and all the available multiwavelength observational data collected during the last two decades by various observers indicates that HD 101584 is most likely a post-AGB star.

The presence of several P-Cygni lines with significant outflow velocities, the OH maser and CO emission profiles (Te Lintel Hekkert et al. 1992, Trams et al. 1990) and the IRAS infrared fluxes and colours (Parthasarathy and Pottasch 1986) indicates the possibility that HD 101584 is a post-AGB star with a bipolar outflow with a dusty disk. Since HD 101584 shows a strong  $H\alpha$  emission line, high resolution imaging with the Hubble Space Telescope (HST) may reveal the bipolar nebula and the presence of a dusty disk similar to that observed in other post-AGB stars like IRAS 17150-3224 (Kwok et al. 1998) or IRAS 17441-2411 (Su et al. 1998).

## References

Bakker E.J., 1994, A&AS 103, 189

Bakker E.J., Lamers H.J.G.L.M., Waters L.B.F.M., Waelkens C., Trams N.R., Van Winckel H., 1996a, A&A 307, 869

Bakker E.J., Lamers H.J.G.L.M., Waters L.B.F.M., Waelkens C., 1996b, A&A 310, 861

Friedjung M., Muratorio G., 1987, A&A, 188, 100

García-Lario P., Parthasarathy M., de Martino D., Monier R., Manchado A., de Córdoba S.F., Pottasch S.R., 1997, A&A, 326, 1103

García-Lario P., Manchado A., Parthasarathy M., Pottasch S.R., 1994, A&A, 285, 179

Hibbert A., Biémont E., Godefroid M., Vaeck N., 1991, A&AS, 88, 505

Hrivnak B., 1997, in Planetary Nebulae, ed. H. J. Habing and H.J.G.M. Lamers, IAU symp. No. 180, 303

Hoffleit D., Saladya M., Wlasuk P., 1983, Supplement to the Bright star Catalogue, Yale University Observatory, USA

Hubeny I., Stefl S., Harmanec P., 1985, Bull. Astron. Inst. Czechosl. 36, 214

Humphreys R.M., 1976, ApJ 206, 122

Humphreys R.M., Ney E.P., 1974, ApJ 190, 339

Kurucz R.L., 1994, Solar Abundance Model Atmospheres, Kurucz CD-ROM No.19, Smithsonian Astrophysical Observatory

Kwok S., Su K.Y.L., Hrivnak B.J., 1998, ApJ, 501, L117

Lang K.R., 1992, Astrophysical data: Planets and stars, Springer Verlag

Morrison N.D., Zimba J.R., 1989, BAAS 21, 1022

Osterbrock D.E., 1989, Astrophysics of Gaseous Nebulae and Active Galactic Nuclei, Oxford University Press, p.117

Parthasarathy M., García-Lario P., Pottasch S.R., 1992, A&A, 264, 159

Parthasarathy M., Pottasch S.R., 1986, A&A, 154, L16

Reddy B.E., Parthasarathy M., Gonzalez G., Bakker E.J., 1997, A&A 328, 331

Rosenzweig P., Reinoso E.G., Naranjo O., 1997, JRASC, 91, 255

Su K.Y.L., Volk K., Kwok S., Hrivnak B.J., 1998, ApJ 508, 744

Te Lintel Hekkert P., Chapman J.M., Zijlstra A.A., 1992, ApJ 390, L23

Trams N.R., Van der Veen W.E.C.J., Waelkens C., Waters L.B.F.M., 1990, A&A 233, 153

Viotti R., 1969, Astrophys. Space Sci. 5, 323

Wiese W.L., Smith M.W., Glennon B.M., Atomic Transition Probabilities, Vol. 1, NSRDS-NBS(U.S.) 4, 1966

Wiese W.L., Martin G.A., Wavelength and Transition Probabilities for Atoms and Atomic Ions, NSRDS-NBS(U.S.), 68, 1980

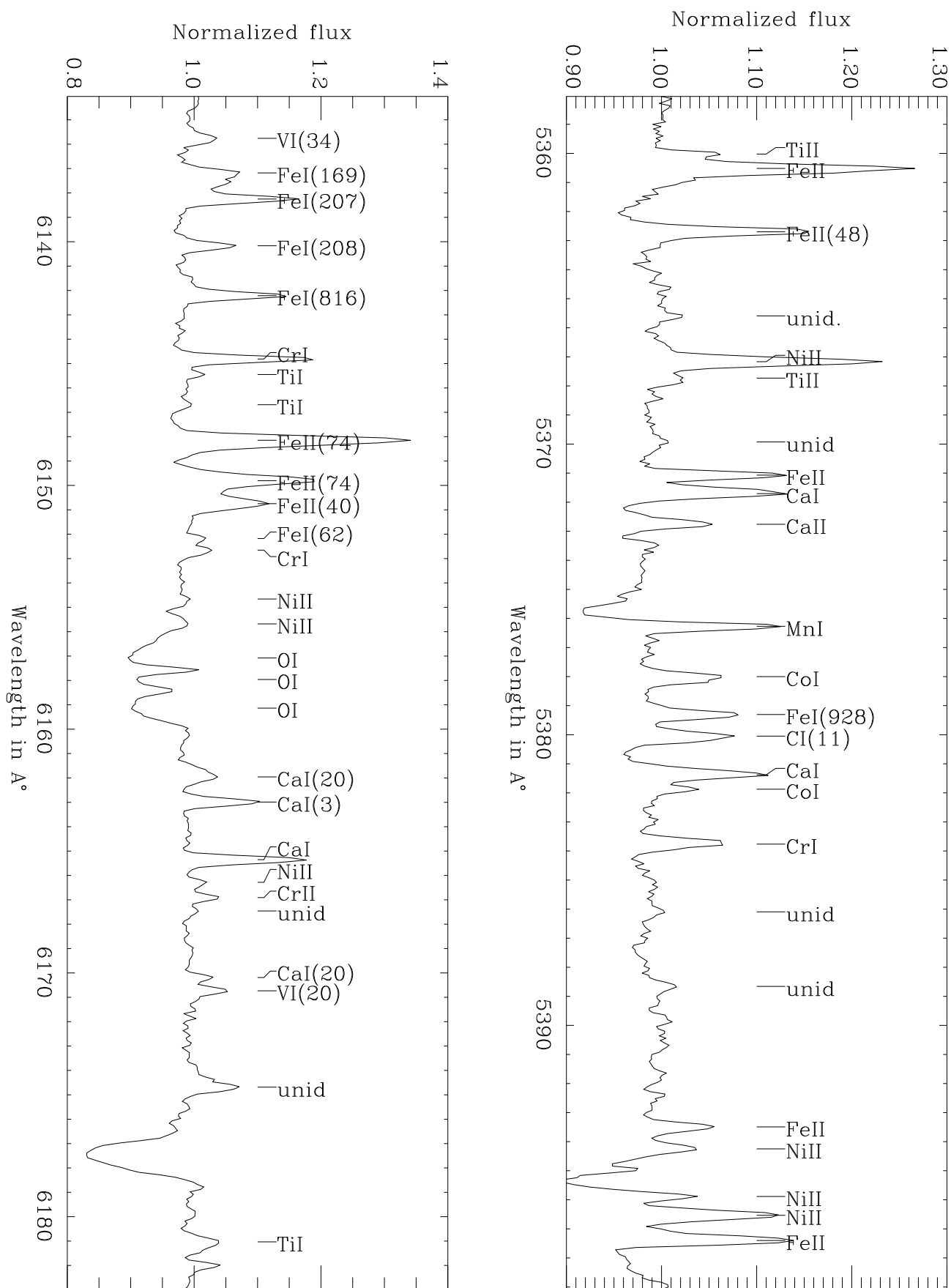


**Fig. 1.** High resolution spectra of HD 101584 obtained with the ESO CAT-CES

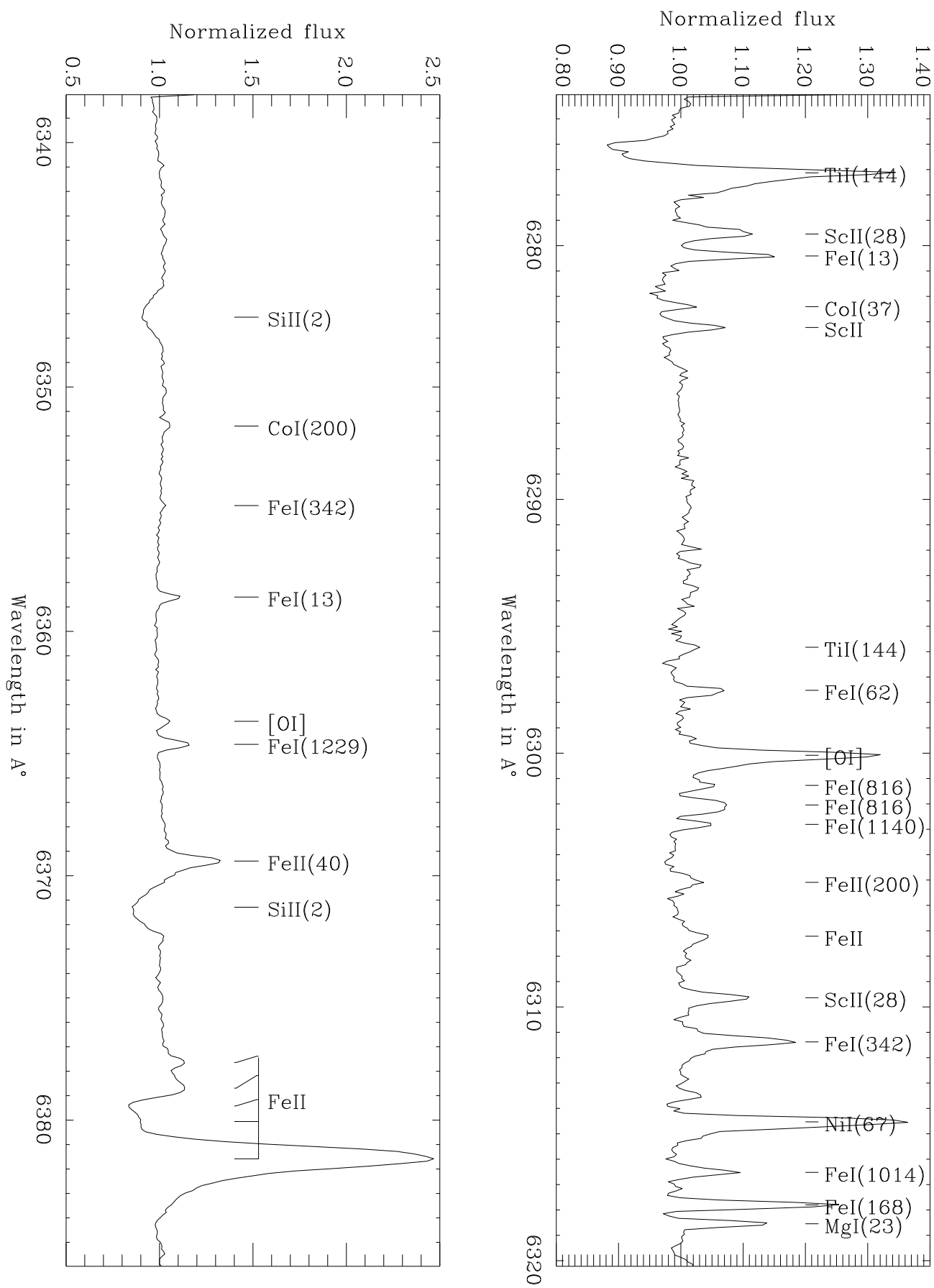


Fig. 1(contd.). High resolution spectra of HD 101584 obtained with the ESO CAT-CES

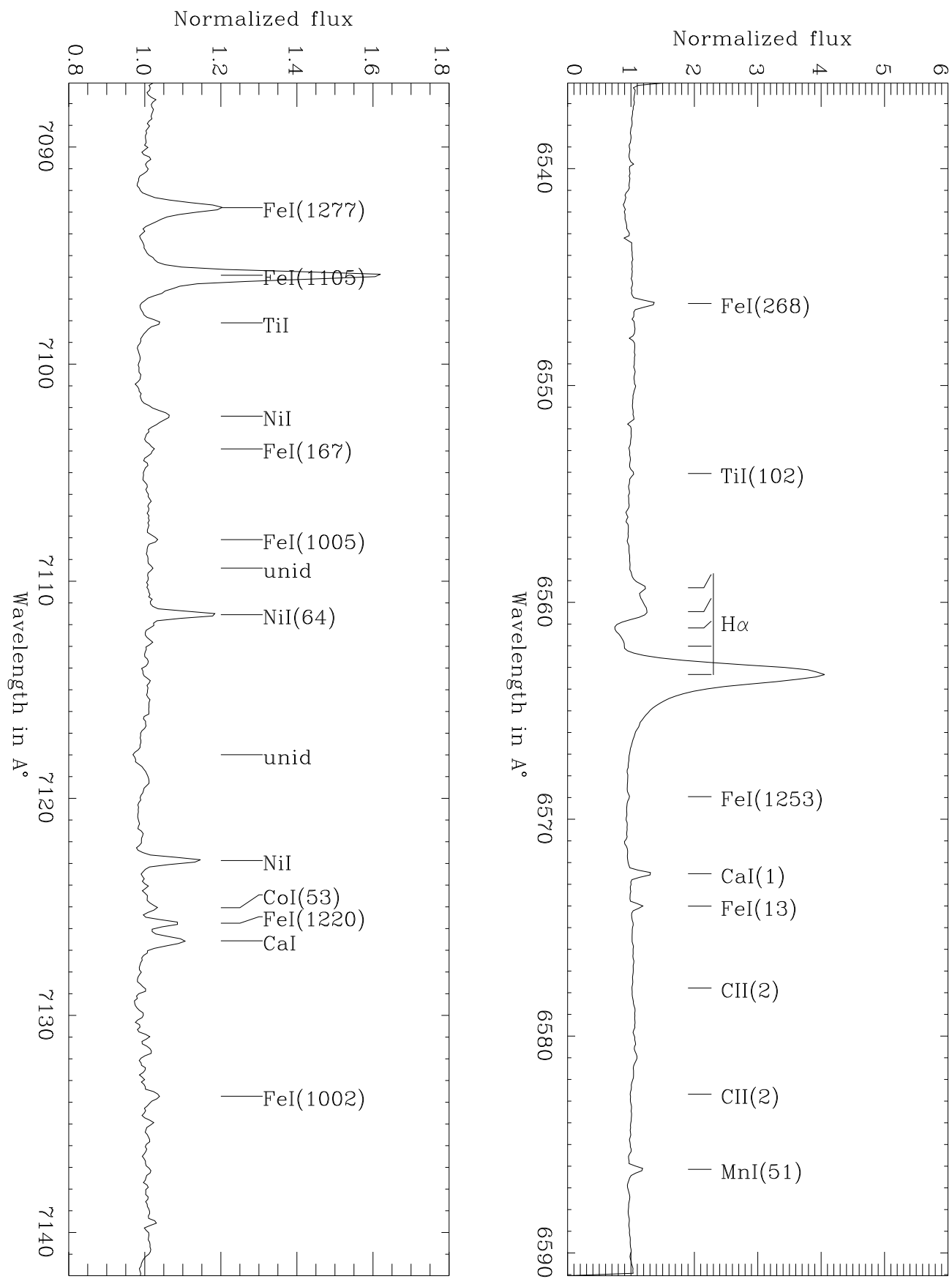


Fig. 1(contd.). High resolution spectra of HD 101584 obtained with the ESO CAT-CES

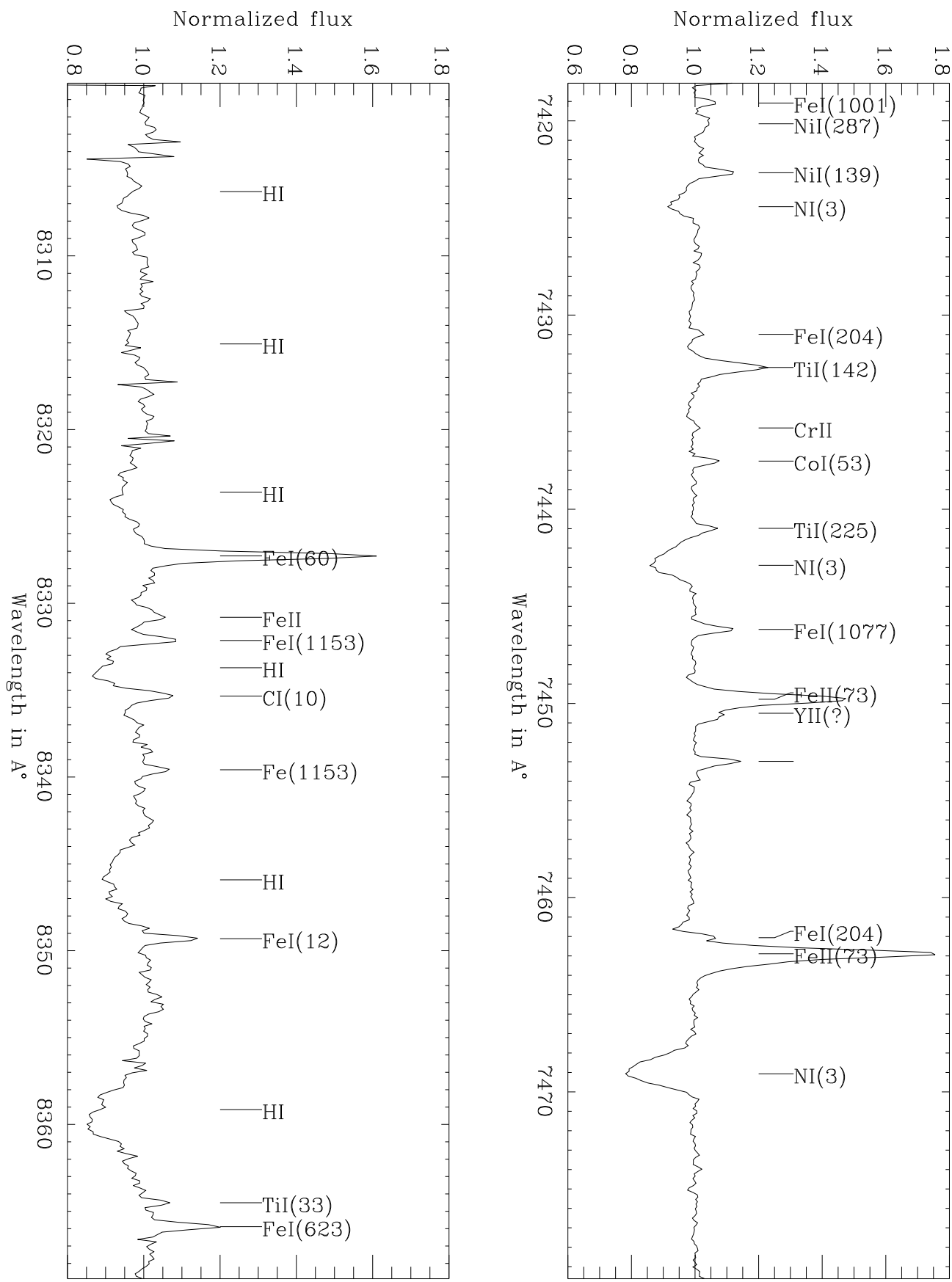


Fig. 1(contd.). High resolution spectra of HD 101584 obtained with the ESO CAT-CES

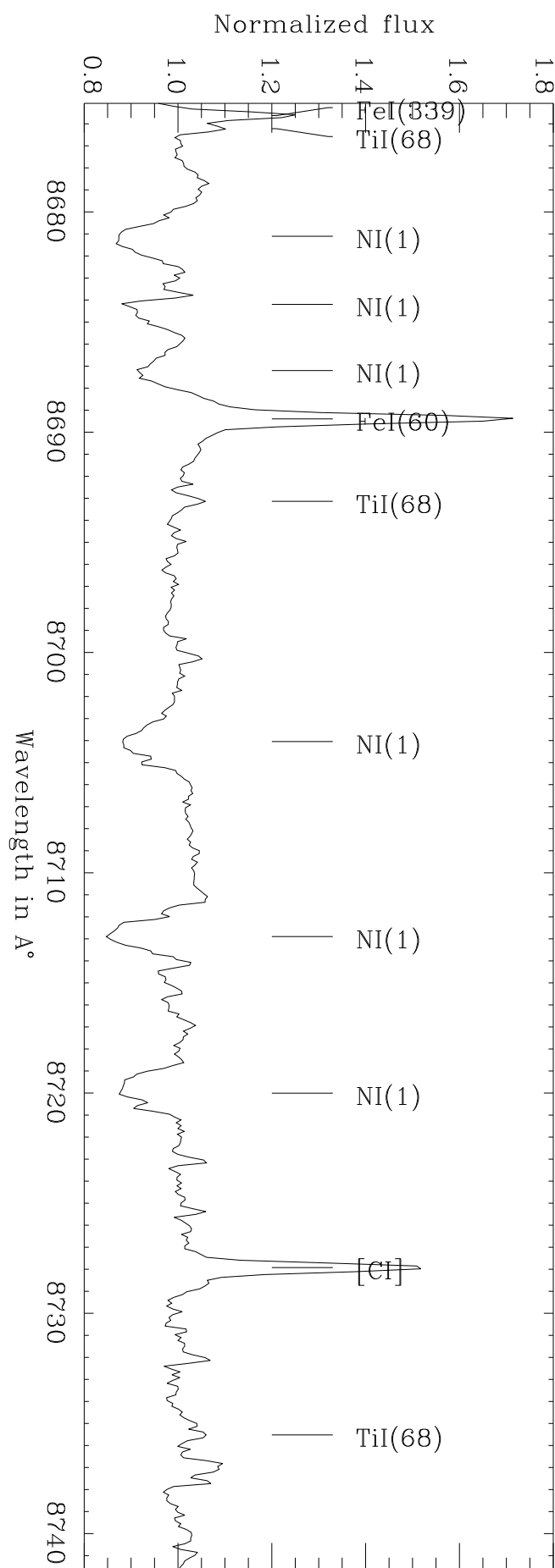
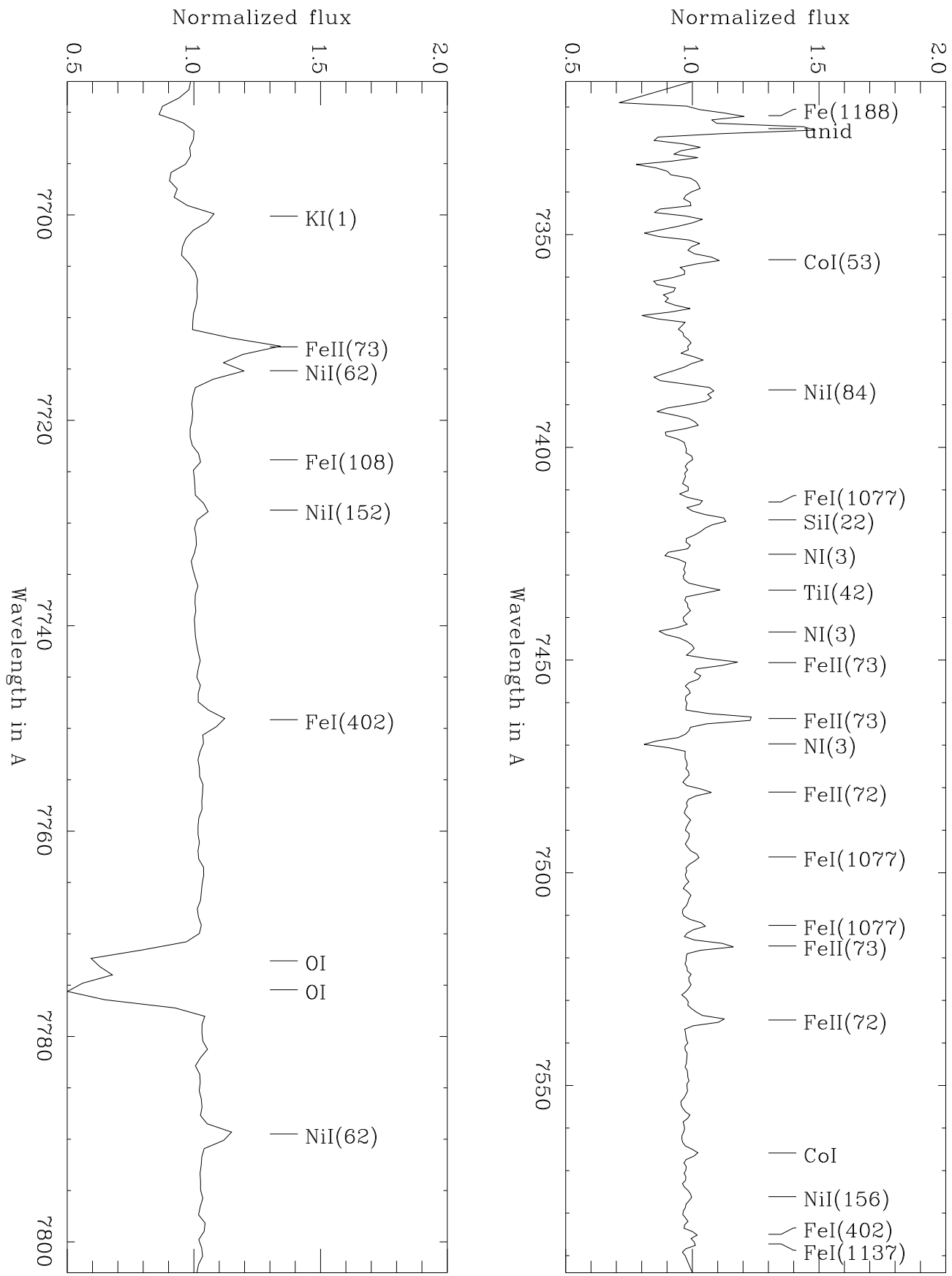
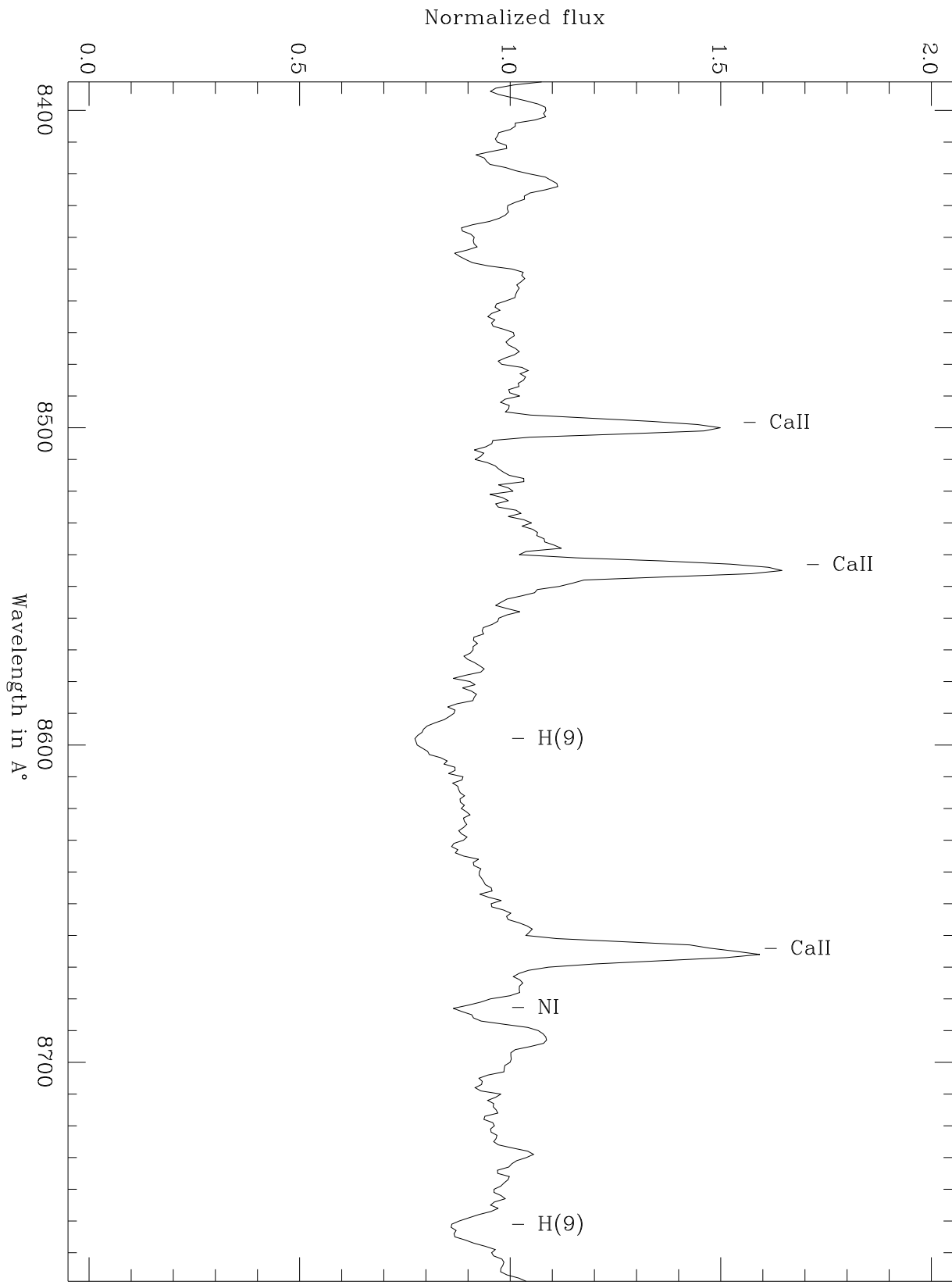


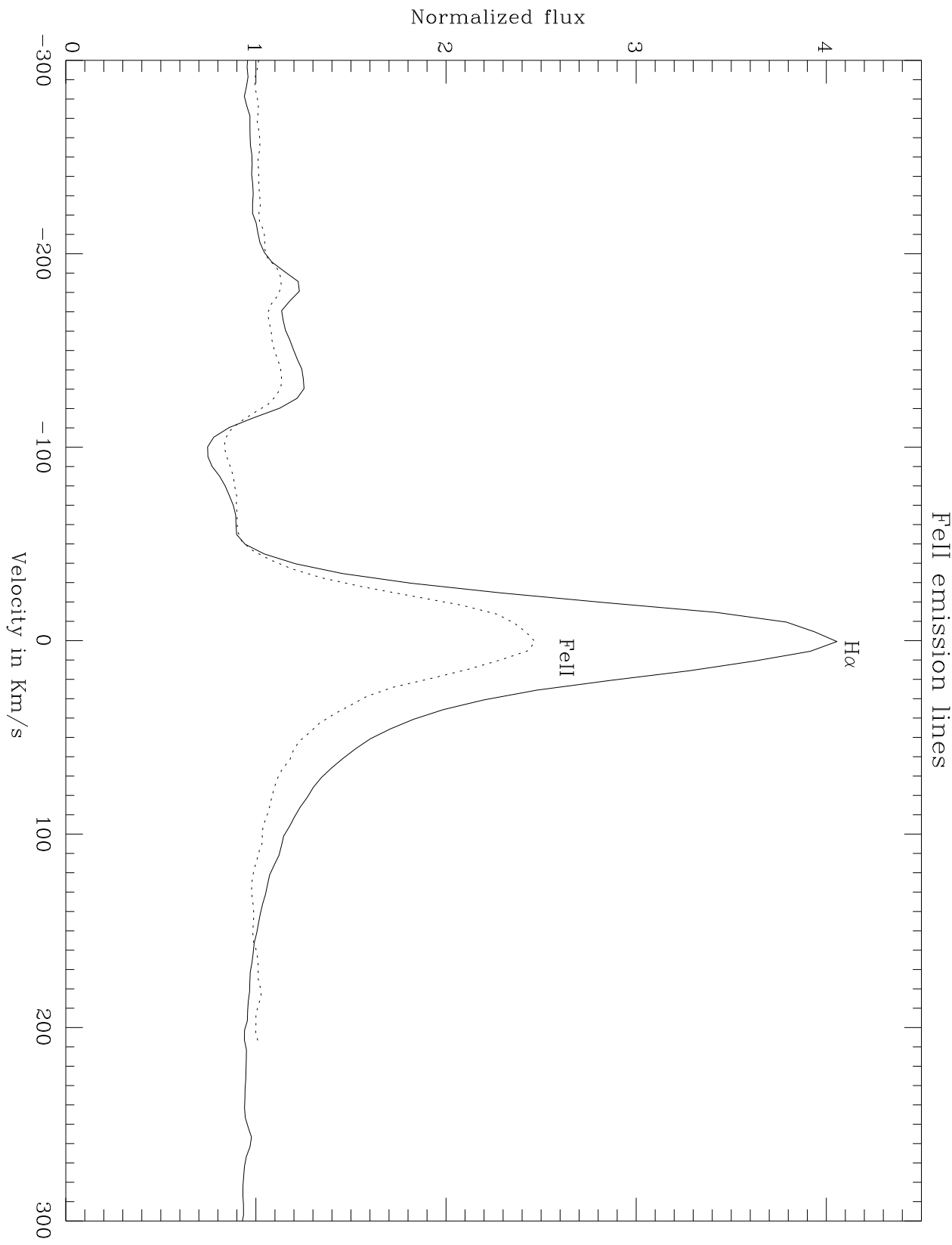
Fig. 1 (contd.). High-resolution spectra of HD 101584 obtained with the ESO CAT CES



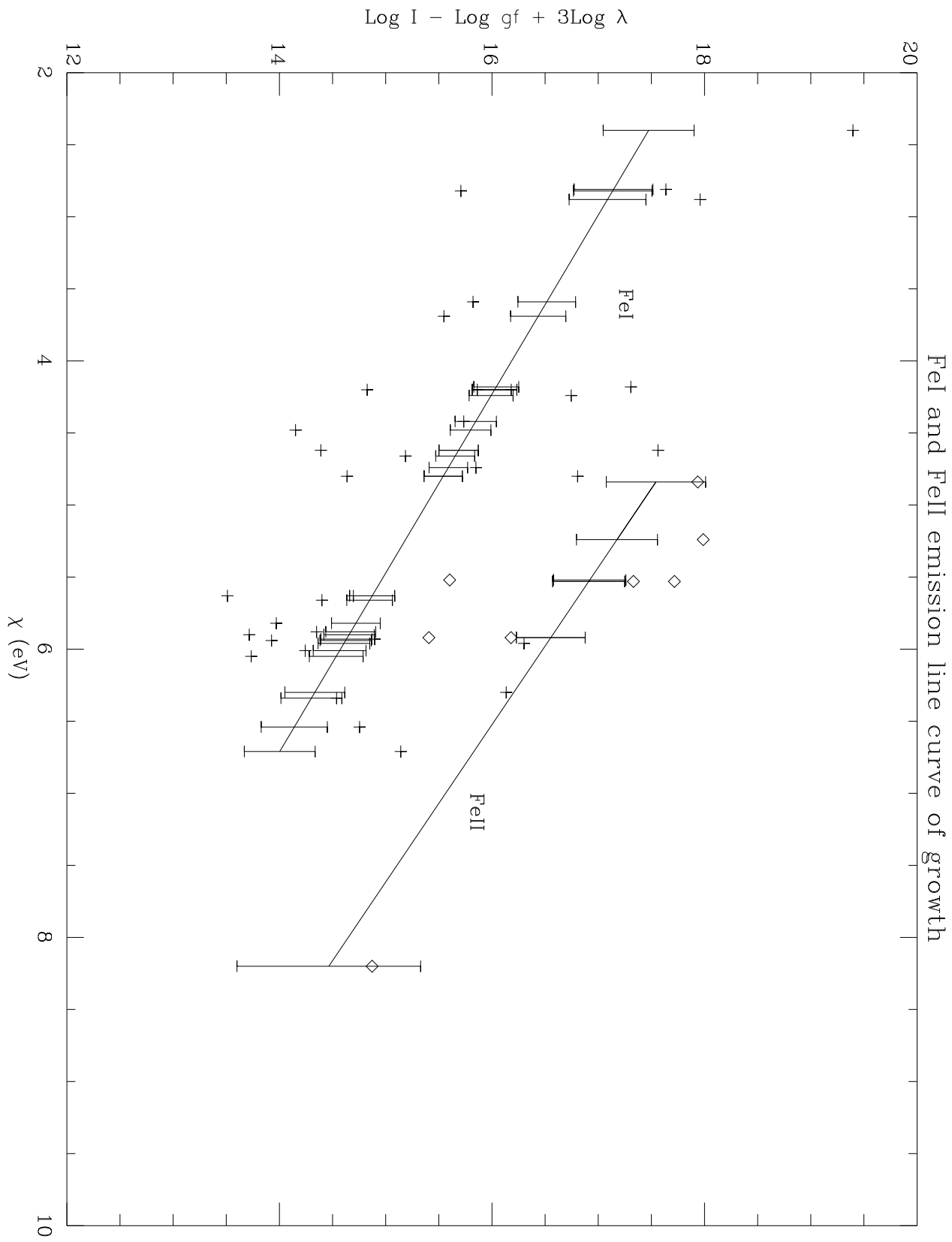
**Fig. 2.** The spectrum in the upper panel shows several nitrogen lines and emission lines of Fe. The lower panel shows the KI 7699 Å in emission and the strong absorption due to OI triplet at 7777 Å.



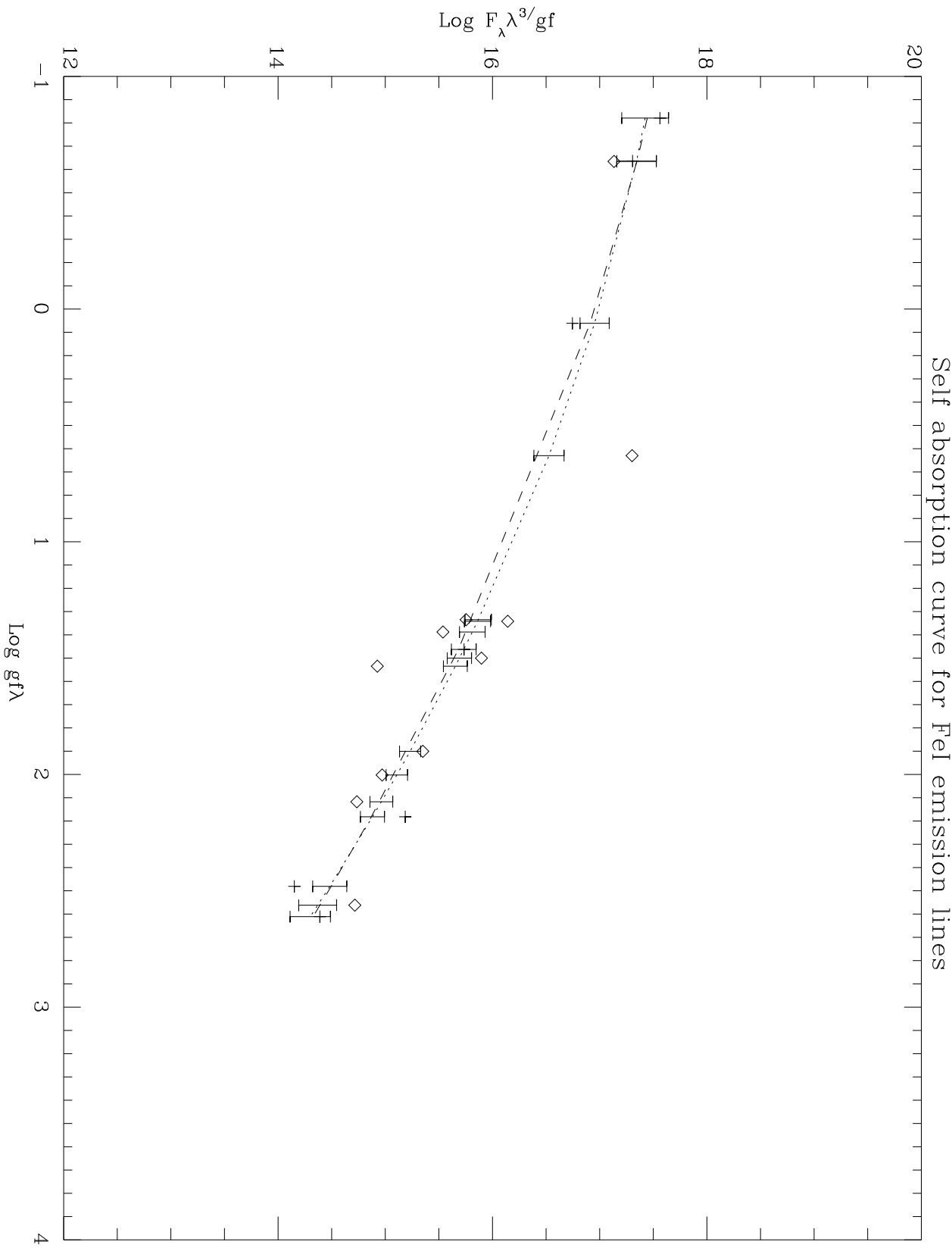
**Fig. 3.** *CaII IR triplet lines showing P-Cygni emission. This spectrum is of  $2.5\text{\AA}$  resolution, obtained from VBO,*



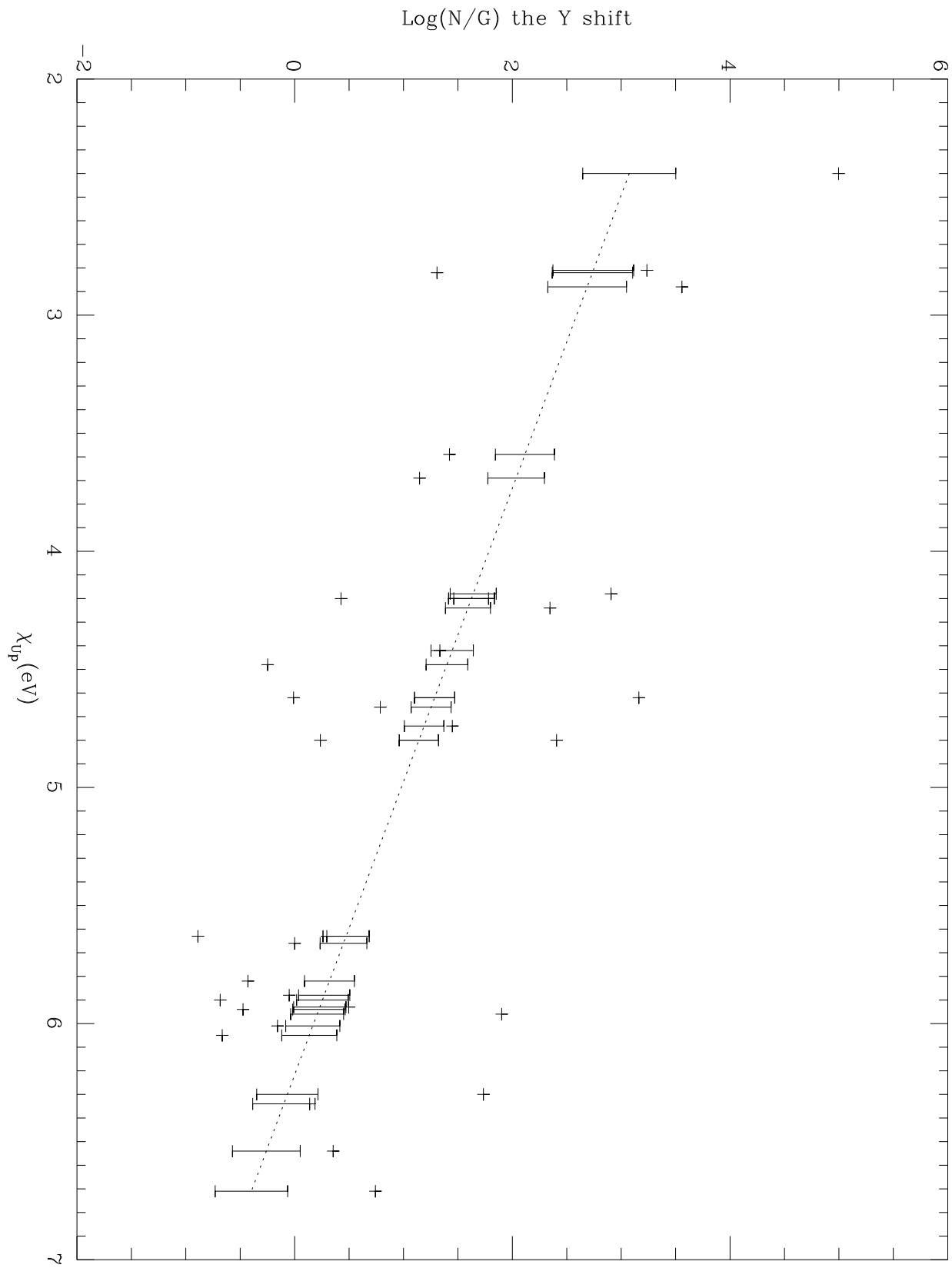
**Fig. 4.** *P-Cygni profile of  $H\alpha$  and FeII(6383Å) lines showing similar velocity structures*



**Fig. 5.** Curve of growth analysis of Fe emission lines. + represents the FeI lines and  $\diamond$  represents FeII lines. The

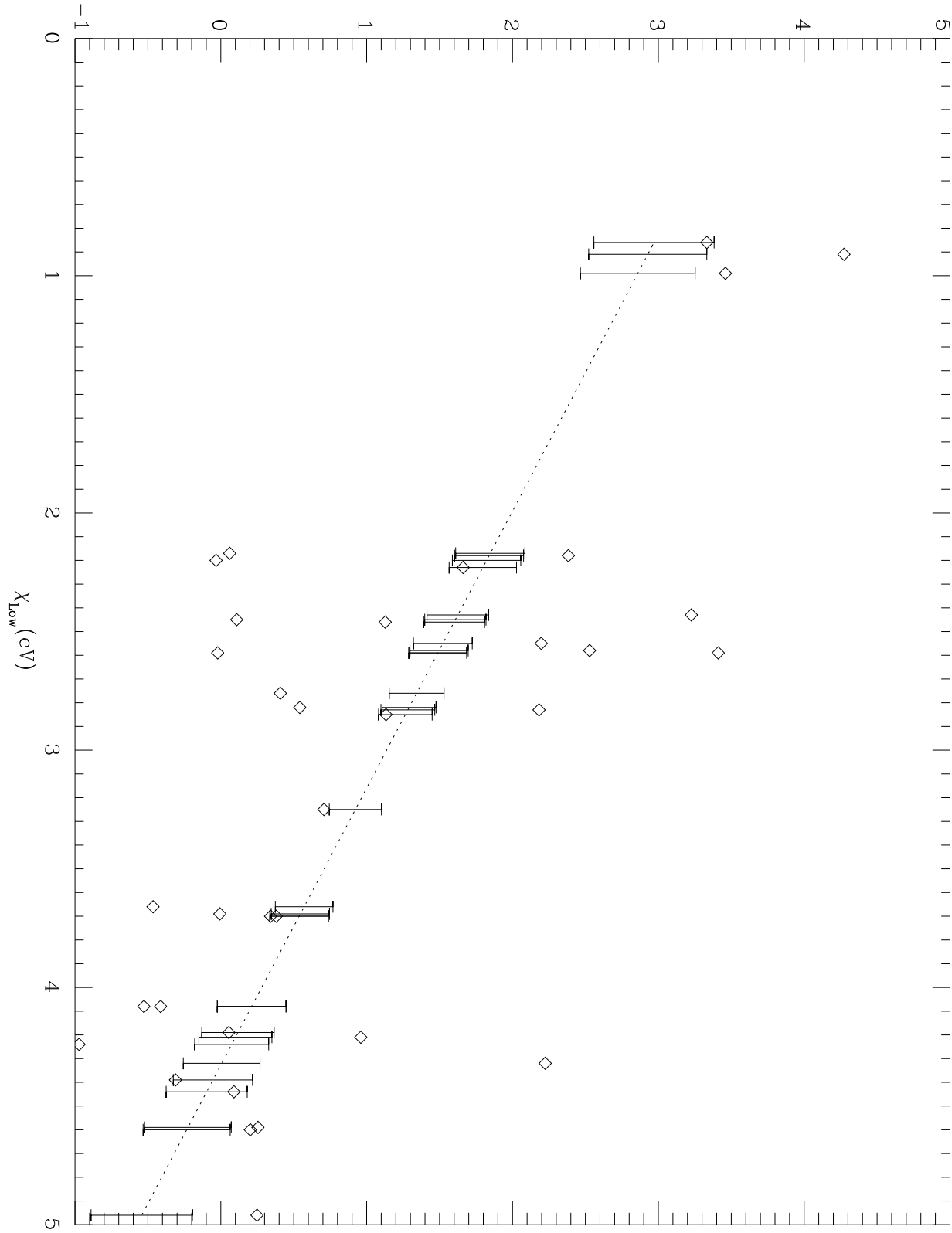


**Fig. 6(a).** The plot shows the shape of the SAC. The + sign indicates multiplets 167, 168, 169, 204, 207, 208 of Fe I having



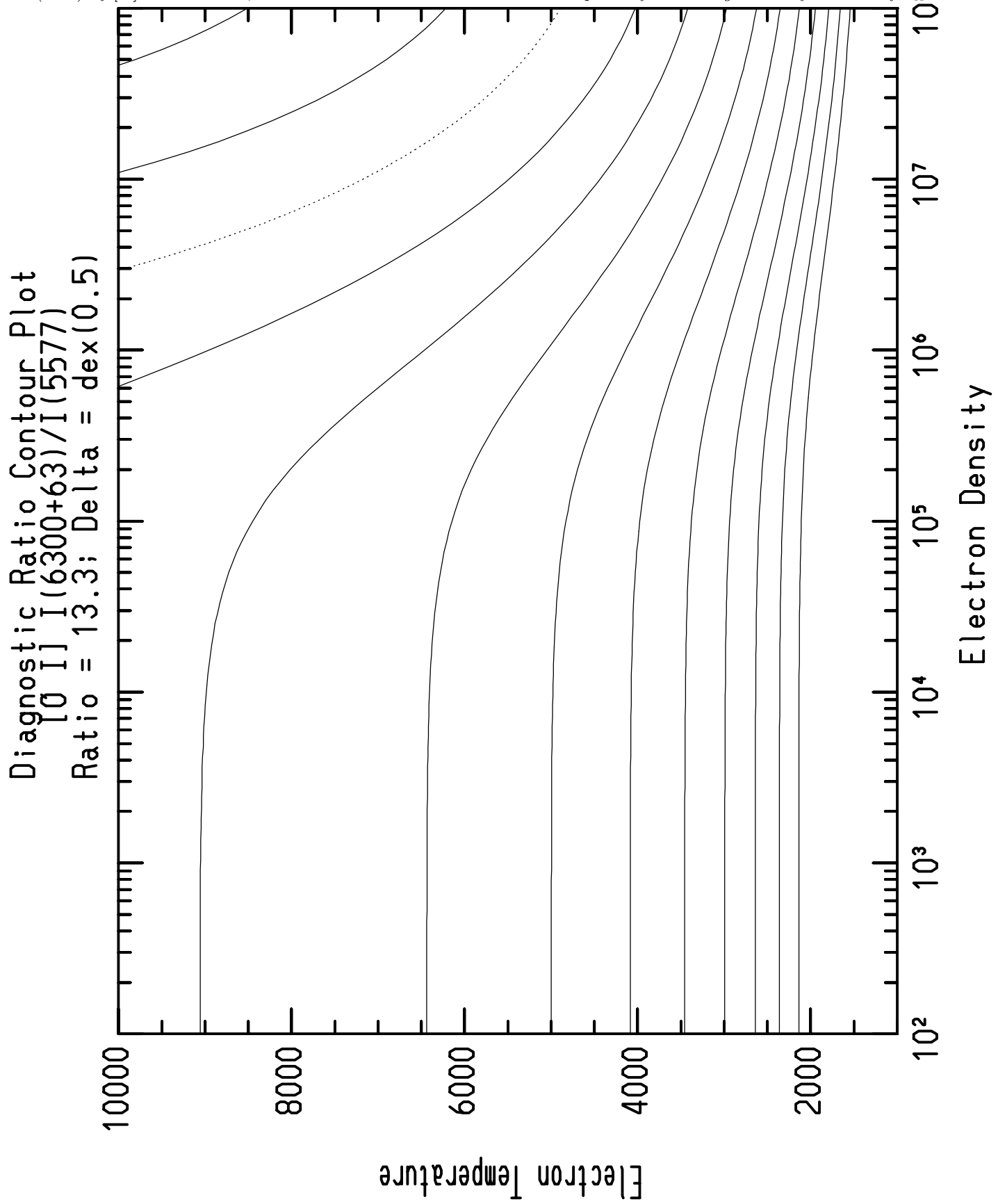
**Fig. 6 (b).** The fit shows the distribution of upper level population of different multiplets of FeI with respect to the

Log(N/G) the X shift



**Fig. 6 (c).** The fit shows the distribution of lower level population of different multiplets of FeI with respect to the

**Fig. 7.** Plot of electron density  $N_e$  and electron temperature  $T_e$ . The dotted line is the contour for the observed ratio (13.3) of [O]I lines 5577Å, 6300Å and 6363Å. Each contour in the plot is for a change in the flux ratio of 0.5.



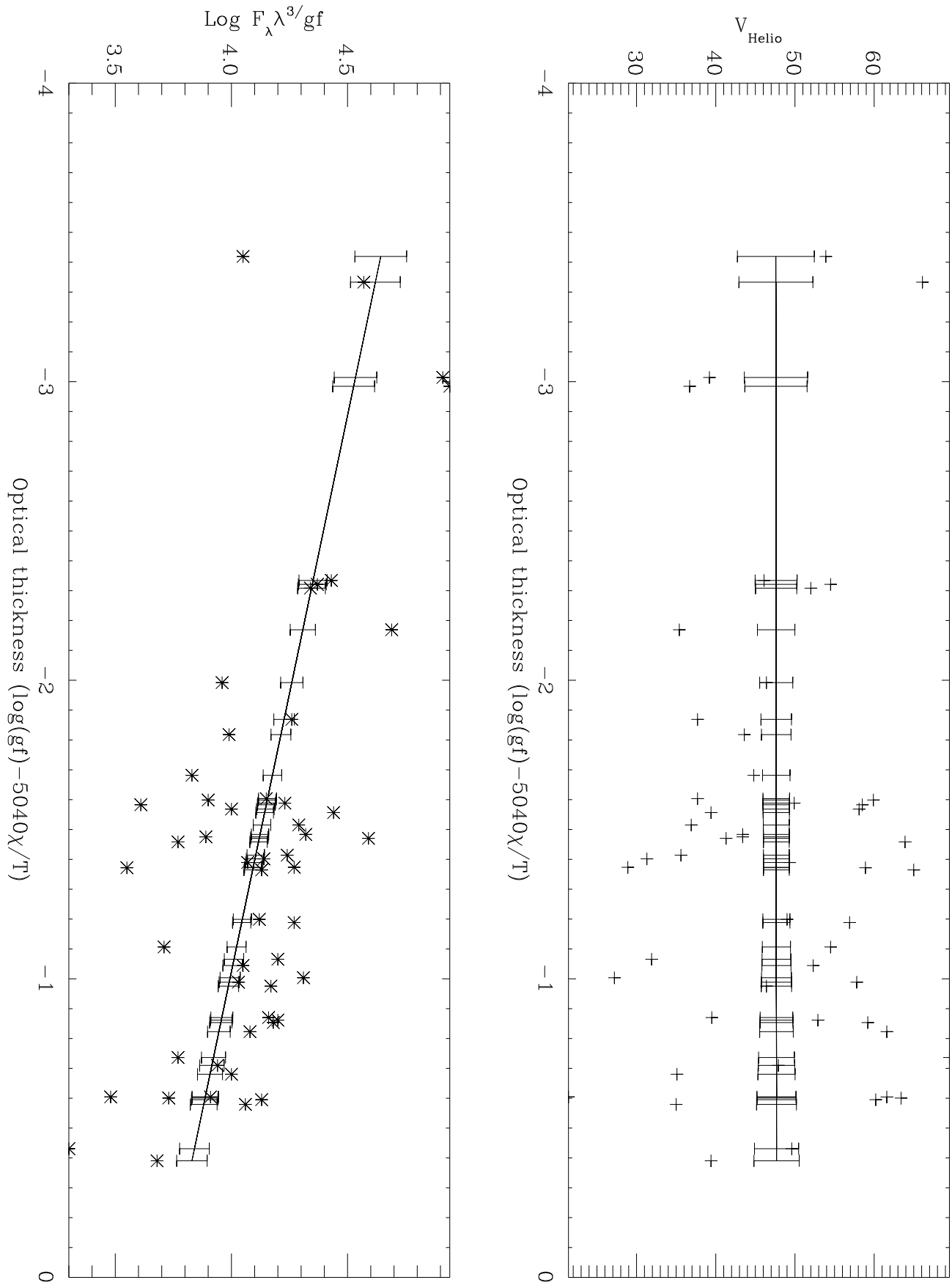


**Fig. 8.** The plot in the upper panel does not show any correlation between the optical depth and the helio centric radial velocity for the Fe I absorption lines of HD 101584 in the wavelength range  $3000\text{ \AA}$ – $5000\text{ \AA}$ . The plot in the lower panel

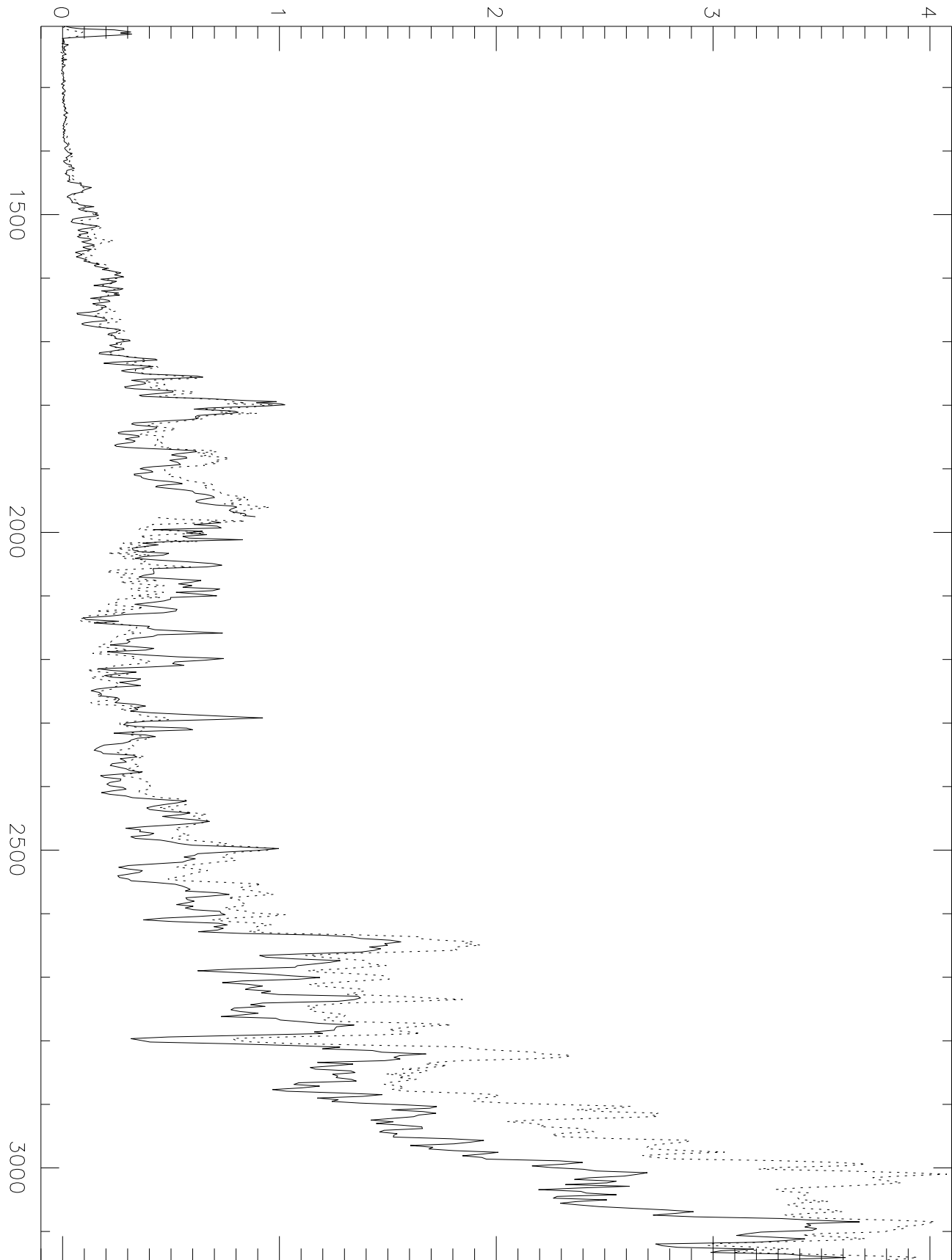


**Fig. 9.** IUE low resolution spectrum of HD 101584 is compared with that of the A6Ia star HD 97534. The dotted line corresponds to the spectrum of HD 97534 while the solid line is HD 101584.

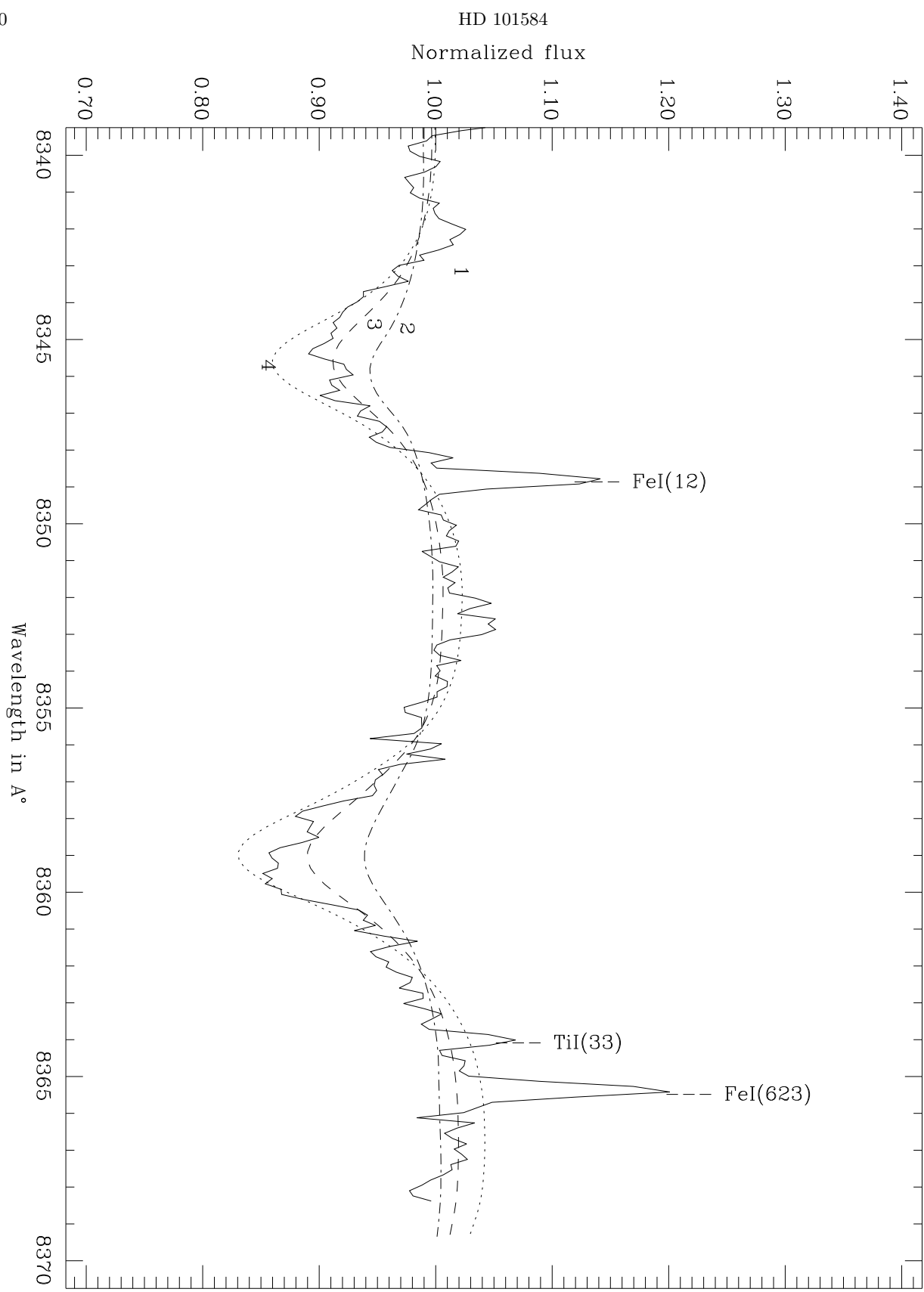


**Fig. 10.** Observed and synthetic spectra in the Paschen line region. 1-observed, 2-Teff=8000K, log g=1.0, 3-

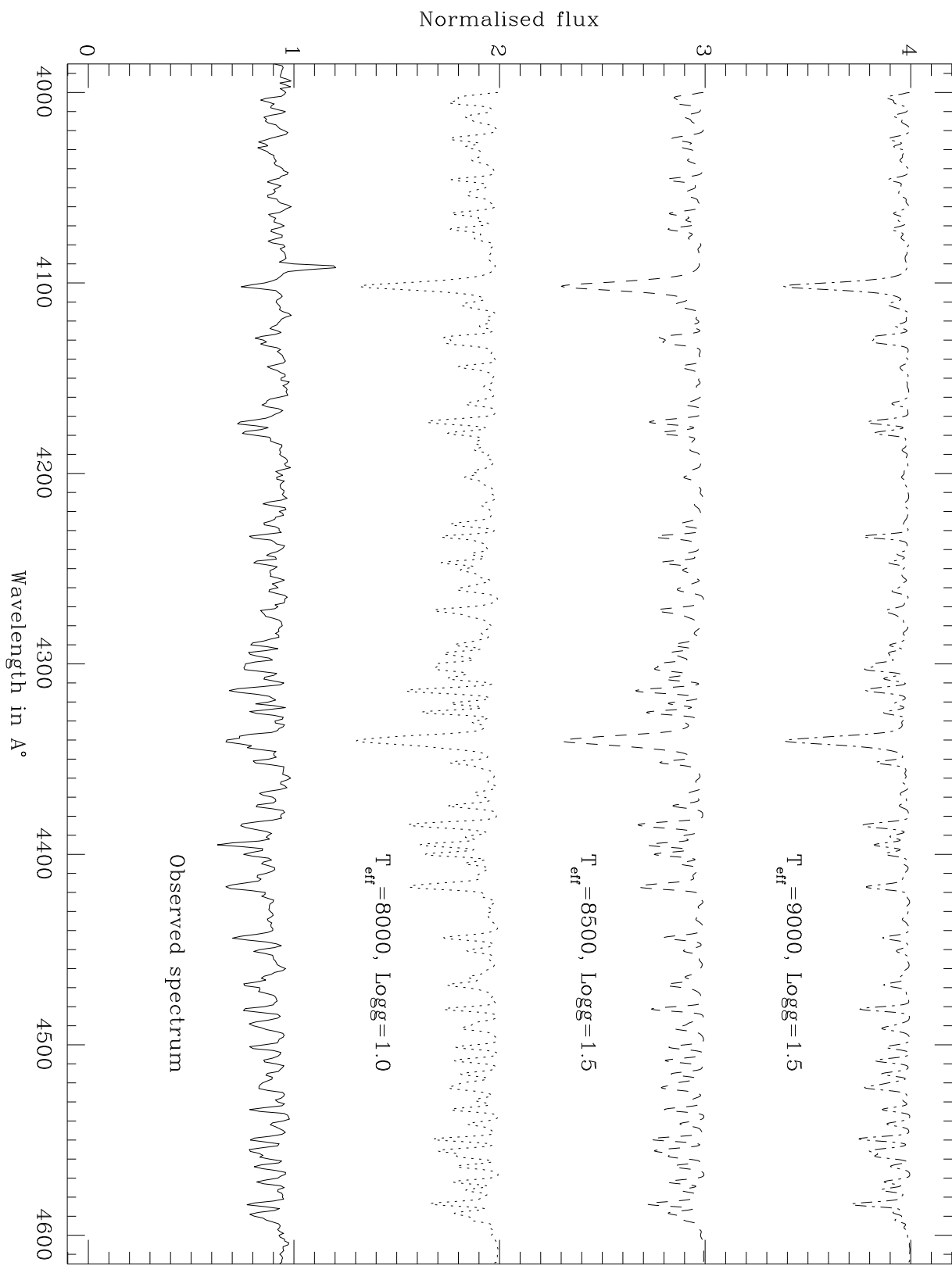


**Fig. 11.** *Synthesis spectra for different models are compared with the observed spectrum. The observed spectrum is of*

Table 1: List of emission lines detected in the high resolution spectrum of HD 10180 (384 ntd.).

of HDS101584	lab	Ident.	$\chi$	log gf	$F_{\lambda}^*$	$\Delta\lambda$	$V_{\text{Helio}}$
AAabs	AAlab	ID	(eV)	log gf	F( $\text{m}\text{\AA}$ )	$\Delta\lambda$ )	Km/s
1460.022	6360.115	T <sub>III</sub>	2.60 $\pm$ 1.92	-4.040	(m $\text{\AA}$ )	(-0.093	10.60s
Table 1: List of emission lines detected in the high-resolution spectrum							
6360.154	6360.353	FeII	70452914283	-0.182	40.84	-0.1237	2.50
6203.828	6203.969	FeII(49)	3.20 $\pm$ 5.52	-2.739	17.36	-0.165	$V_{\text{Helio}}$
6205.594	6207.799	FeI(62)	2.23 $\pm$ 4.20	-2.871	39.23	-0.274	12.91s
6300.065	6300.305	FeII	24601416293	-2.040	163.71	-0.238	15.69
6300.337	6300.503	FeII(816)	3.65 $\pm$ 3.68	-0.780	23.84	-0.287	5.69
6302.008	6302.909	FeI(846)	3.60 $\pm$ 5.66	-1.289	62.86	-0.465	6.565
6303.807	6303.265	FeII(140)	10326613087	-0.435	205.02	-0.633	4.3611
6304.707	6304.904	NaII(200)	6.46 $\pm$ 10.93	-2.033	279.71	-0.228	3.979
6307.761	6307.509	FeII	2.93 $\pm$ 1.80	-1.687	51.64	-0.344	3.697
6309.056	6309.856	SiII(28)	2.93 $\pm$ 4.23	-16.01	55.71	-0.230	4.20
6313.579	6313.295	FeI(342)	10.96 $\pm$ 12.87	-0.920	15.32	-0.246	4.906
6314.504	6314.981	FeI(928)	3.70 $\pm$ 6.01	-1.523	23.83	-0.225	0.43
6316.009	6316.808	ClII(17)	3.10 $\pm$ 6.00	-0.897	13.64	-0.313	0.507
6317.857	6317.599	FeI(1814)	3.99 $\pm$ 5.75	-0.939	39.75	-0.260	3.264
6318.804	6318.645	FeI(284)	3.88 $\pm$ 4.24	-1.81	21.75	-0.491	3.374
6318.865	6318.587	FeI(168)	4.06 $\pm$ 6.84	-3.329	15.82	-0.481	4.799
6319.058	6319.098	FeI(28)	3.10 $\pm$ 6.01	-7.501	31.12	-0.568	6.79
6320.098	6320.098	FeI(200)	7.79 $\pm$ 10.00	-1.810	23.67	-0.273	30.54
6321.421	6321.421	FeI(10)	3.98 $\pm$ 4.92	-2.160	49.97	-0.220	3.752
6322.089	6322.089	FeI(21)	3.58 $\pm$ 6.00	-1.19	17.92	-0.381	3.149
6322.562	6322.562	FeI(18)	3.55 $\pm$ 6.49	-2.254	13.92	-0.370	3.149
6323.700	6323.700	FeI(77)	90.00 $\pm$ 100.00	-0.254	13.64	-0.193	3.176
6326.203	6326.203	FeI(163)	1.54 $\pm$ 1.85	-2.020	48.62	-0.198	3.176
6326.866	6326.866	NaII(3)	1.60 $\pm$ 1.93	-2.120	21.71	-0.164	2.8305
6327.300	6327.300	FeI(13)	0.10 $\pm$ 0.1	65.62	82	-0.14	2.29
6328.039	6328.039	NaI(40)	2.80 $\pm$ 1.93	-2.203	186.78	-0.068	6.4286
6329.008	6329.008	FeI(14F)	10.57 $\pm$ 13.03	-2.283	11.79	-0.210	3.465
6330.610	6330.610	FeI(10)	10.57 $\pm$ 13.03	-74.25	12.87	-0.215	3.469
6331.983	6331.983	FeI(1602)	2.08 $\pm$ 1.84	-1.820	19.61	-0.249	3.4696
6332.806	6332.806	FeI(13)	2.87 $\pm$ 3.81	-8.248	10.13	-0.350	3.632
6333.923	6333.923	FeI(169)	1.94 $\pm$ 2.93	-0.250	40.12	-0.324	6.562
6334.923	6334.923	FeI(60)	2.20 $\pm$ 3.63	-2.98	10.74	-0.214	2.376
6335.802	6335.802	FeI(169)	2.46 $\pm$ 3.63	-6.581	13.79	-0.368	3.1417
6336.496	6336.496	FeI(10)	2.08 $\pm$ 1.84	-74.25	12.87	-0.215	3.465
6337.802	6337.802	FeI(1602)	2.08 $\pm$ 1.84	-1.820	19.61	-0.249	3.4696
6338.806	6338.806	FeI(13)	2.87 $\pm$ 3.81	-8.248	10.13	-0.350	3.632
6339.923	6339.923	FeI(169)	1.94 $\pm$ 2.93	-0.250	40.12	-0.324	6.562
6340.802	6340.802	FeI(169)	2.46 $\pm$ 3.63	-6.581	13.79	-0.368	3.1417
6341.606	6341.606	FeI(10)	2.20 $\pm$ 3.63	-2.98	10.74	-0.214	2.376
6342.606	6342.606	FeI(169)	2.46 $\pm$ 3.63	-6.581	13.79	-0.368	3.1417
6343.606	6343.606	FeI(10)	2.20 $\pm$ 3.63	-2.98	10.74	-0.214	2.376
6344.606	6344.606	FeI(169)	2.46 $\pm$ 3.63	-6.581	13.79	-0.368	3.1417
6345.606	6345.606	FeI(10)	2.20 $\pm$ 3.63	-2.98	10.74	-0.214	2.376
6346.606	6346.606	FeI(169)	2.46 $\pm$ 3.63	-6.581	13.79	-0.368	3.1417
6347.606	6347.606	FeI(10)	2.20 $\pm$ 3.63	-2.98	10.74	-0.214	2.376
6348.606	6348.606	FeI(169)	2.46 $\pm$ 3.63	-6.581	13.79	-0.368	3.1417
6349.606	6349.606	FeI(10)	2.20 $\pm$ 3.63	-2.98	10.74	-0.214	2.376
6350.606	6350.606	FeI(169)	2.46 $\pm$ 3.63	-6.581	13.79	-0.368	3.1417
6351.606	6351.606	FeI(10)	2.20 $\pm$ 3.63	-2.98	10.74	-0.214	2.376
6352.606	6352.606	FeI(169)	2.46 $\pm$ 3.63	-6.581	13.79	-0.368	3.1417
6353.606	6353.606	FeI(10)	2.20 $\pm$ 3.63	-2.98	10.74	-0.214	2.376
6354.606	6354.606	FeI(169)	2.46 $\pm$ 3.63	-6.581	13.79	-0.368	3.1417
6355.606	6355.606	FeI(10)	2.20 $\pm$ 3.63	-2.98	10.74	-0.214	2.376
6356.606	6356.606	FeI(169)	2.46 $\pm$ 3.63	-6.581	13.79	-0.368	3.1417
6357.606	6357.606	FeI(10)	2.20 $\pm$ 3.63	-2.98	10.74	-0.214	2.376
6358.606	6358.606	FeI(169)	2.46 $\pm$ 3.63	-6.581	13.79	-0.368	3.1417
6359.606	6359.606	FeI(10)	2.20 $\pm$ 3.63	-2.98	10.74	-0.214	2.376
6360.606	6360.606	FeI(169)	2.46 $\pm$ 3.63	-6.581	13.79	-0.368	3.1417
6361.606	6361.606	FeI(10)	2.20 $\pm$ 3.63	-2.98	10.74	-0.214	2.376
6362.606	6362.606	FeI(169)	2.46 $\pm$ 3.63	-6.581	13.79	-0.368	3.1417
6363.606	6363.606	FeI(10)	2.20 $\pm$ 3.63	-2.98	10.74	-0.214	2.376
6364.606	6364.606	FeI(169)	2.46 $\pm$ 3.63	-6.581	13.79	-0.368	3.1417
6365.606	6365.606	FeI(10)	2.20 $\pm$ 3.63	-2.98	10.74	-0.214	2.376
6366.606	6366.606	FeI(169)	2.46 $\pm$ 3.63	-6.581	13.79	-0.368	3.1417
6367.606	6367.606	FeI(10)	2.20 $\pm$ 3.63	-2.98	10.74	-0.214	2.376
6368.606	6368.606	FeI(169)	2.46 $\pm$ 3.63	-6.581	13.79	-0.368	3.1417
6369.606	6369.606	FeI(10)	2.20 $\pm$ 3.63	-2.98	10.74	-0.214	2.376
6370.606	6370.606	FeI(169)	2.46 $\pm$ 3.63	-6.581	13.79	-0.368	3.1417
6371.606	6371.606	FeI(10)	2.20 $\pm$ 3.63	-2.98	10.74	-0.214	2.376
6372.606	6372.606	FeI(169)	2.46 $\pm$ 3.63	-6.581	13.79	-0.368	3.1417
6373.606	6373.606	FeI(10)	2.20 $\pm$ 3.63	-2.98	10.74	-0.214	2.376
6374.606	6374.606	FeI(169)	2.46 $\pm$ 3.63	-6.581	13.79	-0.368	3.1417
6375.606	6375.606	FeI(10)	2.20 $\pm$ 3.63	-2.98	10.74	-0.214	2.376
6376.606	6376.606	FeI(169)	2.46 $\pm$ 3.63	-6.581	13.79	-0.368	3.1417
6377.606	6377.606	FeI(10)	2.20 $\pm$ 3.63	-2.98	10.74	-0.214	2.376
6378.606	6378.606	FeI(169)	2.46 $\pm$ 3.63	-6.581	13.79	-0.368	3.1417
6379.606	6379.606	FeI(10)	2.20 $\pm$ 3.63	-2.98	10.74	-0.214	2.376
6380.606	6380.606	FeI(169)	2.46 $\pm$ 3.63	-6.581	13.79	-0.368	3.1417
6381.606	6381.606	FeI(10)	2.20 $\pm$ 3.63	-2.98	10.74	-0.214	2.376
6382.606	6382.606	FeI(169)	2.46 $\pm$ 3.63	-6.581	13.79	-0.368	3.1417
6383.606	6383.606	FeI(10)	2.20 $\pm$ 3.63	-2.98	10.74	-0.214	2.376
6384.606	6384.606	FeI(169)	2.46 $\pm$ 3.63	-6.581	13.79	-0.368	3.1417
6385.606	6385.606	FeI(10)	2.20 $\pm$ 3.63	-2.98	10.74	-0.214	2.376
6386.606	6386.606	FeI(169)	2.46 $\pm$ 3.63	-6.581	13.79	-0.368	3.1417
6387.606	6387.606	FeI(10)	2.20 $\pm$ 3.63	-2.98	10.74	-0.214	2.376
6388.606	6388.606	FeI(169)	2.46 $\pm$ 3.63	-6.581	13.79	-0.368	3.1417
6389.606	6389.606	FeI(10)	2.20 $\pm$ 3.63	-2.98	10.74	-0.214	2.376
6390.606	6390.606	FeI(169)	2.46 $\pm$ 3.63	-6.581	13.79	-0.368	3.1417
6391.606	6391.606	FeI(10)	2.20 $\pm$ 3.63	-2.98	10.74	-0.214	2.376
6392.606	6392.606	FeI(169)	2.46 $\pm$ 3.63	-6.581	13.79	-0.368	3.1417
6393.606	6393.606	FeI(10)	2.20 $\pm$ 3.63	-2.98	10.74	-0.214	2.376
6394.606	6394.606	FeI(169)	2.46 $\pm$ 3.63	-6.581	13.79	-0.368	3.1417
6395.606	6395.606	FeI(10)	2.20 $\pm$ 3.63	-2.98	10.74	-0.214	2.376
6396.606	6396.606	FeI(169)	2.46 $\pm$ 3.63	-6.581	13.79	-0.368	3.1417
6397.606	6397.606	FeI(10)	2.20 $\pm$ 3.63	-2.98	10.74	-0.214	2.376
6398.606	6398.606	FeI(169)	2.46 $\pm$ 3.63	-6.581	13.79	-0.368	3.1417
6399.606	6399.606	FeI(10)	2.20 $\pm$ 3.63	-2.98	10.74	-0.214	2.376
6400.606	6400.606	FeI(169)	2.46 $\pm$ 3.63	-6.581	13.79	-0.368	3.1417
6401.606	6401.606	FeI(10)	2.20 $\pm$ 3.63	-2.98	10.74	-0.214	2.376
6402.606	6402.606	FeI(169)	2.46 $\pm$ 3.63	-6.581	13.79	-0.368	3.1417
6403.606	6403.606	FeI(10)	2.20 $\pm$ 3.63	-2.98	10.74	-0.214	2.376
6404.606	6404.606	FeI(169)	2.46 $\pm$ 3.63	-6.581	13.79	-0.368	3.1417
6405.606	6405.606	FeI(10)	2.20 $\pm$ 3.63	-2.98	10.74	-0.214	2.376
6406.606	6406.606	FeI(169)	2.46 $\pm$ 3.63	-6.581	13.79	-0.368	3.1417
6407.606	6407.606	FeI(10)	2.20 $\pm$ 3.63	-2.98	10.74	-0.214	2.376
6408.606	6408.606	FeI(169)	2.46 $\pm$ 3.63	-6.581	13.79	-0.368	3.1417
6409.606	6409.606	FeI(10)	2.20 $\pm$ 3.63	-2.98	10.74	-0.214	2.376
6410.606	6410.606	FeI(169)	2.46 $\pm$ 3.63	-6.581	13.79	-0.368	3.1417
6411.606	6411.606	FeI(10)	2.20 $\pm$ 3.63	-2.98	10.74	-0.214	2.376
6412.606	6412.606	FeI(169)	2.46 $\pm$ 3.63	-6.581	13.79	-0.368	3.1417
6413.606	6413.606	FeI(10)	2.20 $\pm$ 3.63	-2.98	10.74	-0.214	2.376
6414.606	6414.606	FeI(169)	2.46 $\pm$ 3.63	-6.581	13.79	-0.368	3.1417
6415.606	6415.606	FeI(10)	2.20 $\pm$ 3.63	-2.98	10.74	-0.214	2.376
6416.606	6416.606	FeI(169)	2.46 $\pm$ 3.63	-6.581	13.79	-0.368	3.1417
6417.606	6417.606	FeI(10)	2.20 $\pm$ 3.63	-2.98	10.74	-0.214	2.376
6418.606	6418.606	FeI(169)	2.46 $\pm$ 3.63	-6.581	13.79	-0.368	

Table 1 (contd.): List of emission lines detected in the high resolution spectrum of HD 101584

$\lambda$ obs (Å)	$\lambda$ lab (Å)	ID	$\chi$ (eV)	log gf	$F_\lambda^*$ (mÅ)	$\Delta\lambda$ (Å)	$V_{Helio}$ km/s
6283.225	6283.353	ScII	7.45-9.43	-0.441	40.34	-0.127	9.90
6295.826	6295.949	TiI(144)					
6297.524	6297.799	FeI(62)	2.23-4.20	-2.871	39.23	-0.274	2.91
6300.083	6300.311	[OI]			163	-0.228	5.15
6301.27	6301.508	FeI(816)	3.66-5.63	-0.745	23.32	-0.237	4.68
6302.042	6302.499	FeI(816)	3.69-5.66	-1.203	62.88	-0.457	-5.75
6302.807	6303.461	FeI(1140)	4.32-6.30	-3.434	20.01	-0.653	-15.11
6305.09	6305.314	FeII(200)	6.23-8.20	-2.039	27.17	-0.224	5.34
6307.214	6307.529	FeII	2.83-4.80	-5.685	57.4	-0.314	1.02
6309.636	6309.886	ScII(28)	1.5-3.47	-1.630	55.71	-0.250	4.12
6311.379	6311.504	FeI(342)	2.83-4.80	-3.392	103.2	-0.125	10.06
6313.52							
6314.529	6314.668	NiI(67)	4.16-6.13	-0.921	163.5	-0.139	9.39
6316.52	6315.814	FeI(1014)	4.08-6.05	-0.683	44.72	0.706	49.54
6317.802	6318.027	FeI(168)	2.46-4.42	-2.338	98.8	-0.181	7.40
6318.545	6318.717	MgI(23)	5.12-7.08	-1.730	60.1	-0.171	7.84
6351.598	6351.448	CoI(200)					
6354.852	6355.027	FeI(342)	2.85-4.80	-2.346	7.6	-0.174	7.62
6358.596	6358.687	FeI(13)	0.86-2.81	-4.546	47.9	-0.0908	11.59
6363.68	6363.79	[OI]			28.9	-0.109	10.69
6364.625	6364.706	FeI(1229)	4.59-6.54	-1.469	74.78	-0.081	12.05
6369.4	6369.464	FeII(40)	2.89-4.84	-4.253	186.8	-0.063	12.86
6380.058	6383.715	FeII	5.56-7.50	-2.271	1512	-3.656	-155.97
6381.582	6381.416	TiI(196)					
6539.783	6539.72	FeI(405)					
6546.217	6546.245	FeI(268)	2.76-4.66	-1.634	127.2	-0.0283	14.97
6554.056	6554.226	TiI(102)	1.44-3.34	-1.201	32.48	-0.169	8.49
6561.179	6561.179	H $\alpha$			3681		
6563.326	6563.403	CoI(80)					
6568.959	6569.231	FeI(1253)					
6572.512	6572.779	CaI(1)	0.00-1.89	-4.104	124.5	-0.266	4.10
6574.009	6574.238	FeI(13)	0.99-2.88	-4.688	65.55	-0.229	5.82
6574.831	6575.022	FeI(207)					
6580.992	6581.220	FeI(34)					
6586.144	6586.343	MnI(51)					
6587.438	6587.75	CI(22)					
7092.793	7091.942	FeI(1277)	4.96-6.71	-1.509	120.4	0.886	53.22
7095.905	7095.425	FeI(1105)	4.21-5.96	-2.221	337.4	0.479	36.21
7098.1	7097.655	TiI	3.30-5.30	-3.423	16.88	0.445	34.74
7102.397	7101.932	NiI	4.54-6.29	-1.941	53.25	0.464	35.55
7103.904	7103.15	FeI(167)	2.43-4.18	-4.488	18.39		
7108.084	7107.468	FeI(1005)	4.19-5.94	-1.317	11.32	0.449	34.87
7109.397	7109.397	unid			8.62		
7111.541	7110.905	NiI(64)	1.93-3.68	-3.042	70.85	0.648	43.29
7117.991	7117.991	unid			23.54		
7122.867	7122.191	NiI(126)	3.54-5.29	-0.169	55.08	0.676	44.40
7125.038	7124.47	CoI(53)			14.34		
7125.752	7125.283	FeI(1220)	4.60-6.34	-1.465	32.71	0.468	35.65
7126.566	7126.19	CaI	6.02-7.77	-0.647	60.47	0.375	31.74
7419.082	7418.668	FeI(1001)	4.12-5.79	-1.17	107.8	0.414	32.62
7420.15	7419.31	NiI(287)	5.50-7.17	-0.695		0.839	49.84
7422.671	7422.30	NiI(139)	3.69-5.28	+0.06	57.36	0.371	30.88

Table 1 (contd.): List of emission lines detected in the high resolution spectrum of HD 101584

$\lambda$ obs (Å)	$\lambda$ lab (Å)	ID	$\chi$ (eV)	log gf	$F_{\lambda}^*$ (mÅ)	$\Delta\lambda$ (Å)	$V_{Helio}$ km/s
7430.991	7430.5	FeI(204)	2.58-4.24	-3.81	21.02	0.491	35.71
7432.698	7431.97	TiI(142)	1.74-3.41	-2.283	15.53	0.728	45.27
7435.814	7435.3	unid			47.41		
7437.521	7437.16	CoI(53)	1.95-3.61	-3.64	45.96	0.360	30.43
7440.984	7440.6	TiI(225)	2.25-3.90	-1.19	38.7	0.383	31.35
7446.188	7445.70	FeI(1077)	4.24-5.90	-0.31	61.72	0.487	35.53
7449.784	7449.34	FeII(73)	3.87-5.53	-3.60	316.5	0.444	33.77
7450.505	7450.33	YII(?)			0.174		22.92
7452.982	7452.50	FeII(14F)			54.88		
7462.061	7461.527	FeI(204)	2.55-4.20	-3.48		0.534	37.36
7462.889	7462.38	FeII(73)	3.87-5.53	-2.98	540.5	0.509	36.35
8327.273	8327.061	FeI(60)	2.20-3.69	-1.298	307.8	0.212	23.79
8330.807	8330.587	unid			55.59		
8332.142	8331.926	FeI(1153)	4.39-5.88	-1.020	36.98	0.215	23.89
8335.342	8335.150	CI(10)	7.70-9.19	-0.420	69.24	0.191	23.01
8339.584	8339.398	Fe(1153)	4.44-5.93	-1.421	51.58	0.185	22.80
8349.31	8349.02	FeI(12)	0.91-2.40	-5.605	106.4	0.290	26.54
8364.508	8364.243	TiI(33)	0.83-2.32	-1.652	28.96	0.264	25.61
8365.885	8365.642	FeI(623)	3.25-4.74	-2.040	110.0	0.243	24.84
8675.626	8674.751	FeI(339)	2.82-2.42	-1.89	100.7	0.875	46.10
8676.22	8675.38	TiI(68)	1.06-2.50	-1.357	43.2	0.839	44.88
8689.396	8688.632	FeI(60)	2.17-3.59	-1.41	393.9	0.764	42.24
8693.139	8692.34	TiI(68)	1.04-2.46	-1.92	27.48	0.798	43.41
8727.923	8727.4	[CI]			302.5	0.522	33.80
8735.521	8734.70	TiI(68)	1.05-2.48	-2.087		0.821	44.05

Table 2: Chemical composition of HD101584.

Element	[element/H]		Lines
	$T_{eff}=8500K$ $\log g=1.5$	$T_{eff}=9000K$ $\log g=1.5$	
C	1.0±0.1	0.3±0.1	C II 6578,6582
N	0.5±0.1	0.6±0.1	N I 7423,7442,8703, 8711,8718,8728
O	0.1	0.18	O I 6158
Mg <sup>1</sup>	0.2	0.02	Mg II 4481.13
Ti <sup>1</sup>	0.0±0.4	0.4±0.4	Ti II 15 lines
Fe <sup>1</sup>	-0.1±0.1	0.5±0.1	Fe I 3 lines
	0.2±0.4	0.3±0.4	Fe II 6lines